Microbiological Research 277 (2023) 127498

Contents lists available at ScienceDirect

Microbiological Research

journal homepage: www.elsevier.com/locate/micres

Molecular insights into RmcA-mediated c-di-GMP consumption: Linking redox potential to biofilm morphogenesis in Pseudomonas aeruginosa

Chiara Scribani Rossi [a], Kelly Eckartt [b], Elisabetta Scarchilli [a], Simone Angeli [a], Alexa Price-Whelan [b], Adele Di Matteo [c], Maelenn Chevreuil [d], Bertrand Raynal [d], Alessandro Arcovito [e,f], Noah Giacon [e], Francesco Fiorentino [g], Dante Rotili [g], Antonello Mai [g], Manuel Espinosa-Urgel [h], Francesca Cutruzzolà [a], Lars E.P. Dietrich [b], Alessio Paone [a], Alessandro Paiardini [a], Serena Rinaldo [a,*]

[a] *Laboratory affiliated to Istituto Pasteur Italia, Fondazione Cenci Bolognetti, Department of Biochemical Sciences "A. Rossi Fanelli", Sapienza University of Rome, Rome, Italy*
[b] *Department of Biological Sciences, Columbia University, New York, USA*
[c] *CNR Institute of Molecular Biology and Pathology, I-00185 Rome, Italy*
[d] *Plate-forme de Biophysique Moléculaire, Institut Pasteur, UMR 3528 CNRS, Paris, France*
[e] *Dipartimento di Scienze Biotecnologiche Di Base, Cliniche Intensivologiche e Perioperatorie Università Cattolica Del Sacro Cuore, Roma, Italy*
[f] *Fondazione Policlinico Universitario A. Gemelli – IRCCS, Rome, Italy*
[g] *Department of Drug Chemistry and Technologies, Sapienza University of Rome, Rome, Italy*
[h] *Department of Biotechnology and Environmental Protection. Estación Experimental del Zaidin, CSIC, Granada, Spain*

ARTICLE INFO

Keywords:
C-di-GMP
Phenazine
Phosphodiesterase
Arginine
Biofilm
Signal transduction

ABSTRACT

The ability of many bacteria to form biofilms contributes to their resilience and makes infections more difficult to treat. Biofilm growth leads to the formation of internal oxygen gradients, creating hypoxic subzones where cellular reducing power accumulates, and metabolic activities can be limited. The pathogen Pseudomonas aeruginosa counteracts the redox imbalance in the hypoxic biofilm subzones by producing redox-active electron shuttles (phenazines) and by secreting extracellular matrix, leading to an increased surface area-to-volume ratio, which favors gas exchange. Matrix production is regulated by the second messenger bis-(3′,5′)-cyclic-dimeric-guanosine monophosphate (c-di-GMP) in response to different environmental cues. RmcA (Redox modulator of c-di-GMP) from P. aeruginosa is a multidomain phosphodiesterase (PDE) that modulates c-di-GMP levels in response to phenazine availability. RmcA can also sense the fermentable carbon source arginine via a periplasmic domain, which is linked via a transmembrane domain to four cytoplasmic Per-Arnt-Sim (PAS) domains followed by a diguanylate cyclase (DGC) and a PDE domain. The biochemical characterization of the cytoplasmic portion of RmcA reported in this work shows that the PAS domain adjacent to the catalytic domain tunes RmcA PDE activity in a redox-dependent manner, by differentially controlling protein conformation in response to FAD or FADH2. This redox-dependent mechanism likely links the redox state of phenazines (via FAD/FADH2 ratio) to matrix production as indicated by a hyperwrinkling phenotype in a macrocolony biofilm assay. This study provides insights into the role of RmcA in transducing cellular redox information into a structural response of the biofilm at the population level. Conditions of resource (i.e. oxygen and nutrient) limitation arise during chronic infection, affecting the cellular redox state and promoting antibiotic tolerance. An understanding of the molecular linkages between condition sensing and biofilm structure is therefore of crucial importance from both biological and engineering standpoints.

1. Introduction

Bacteria can switch their lifestyle in response to environmental conditions from a free-living planktonic entity to a multicellular aggregate, held together by a self-produced matrix, called biofilm. The physiological re-programming required to promote biofilm formation or

* Correspondence to: Dept. of Biochemical Sciences University of Rome "La Sapienza"P.le Aldo Moro, 5 - 00185 Rome
E-mail address: serena.rinaldo@uniroma1.it (S. Rinaldo).

https://doi.org/10.1016/j.micres.2023.127498

Available online 15 September 2023

dispersion is controlled by intracellular variation of the second messenger bis-(3′,5′)-cyclic-dimeric-guanosine (c-di-GMP) (Rinaldo et al., 2015; Römling et al., 2017). High c-di-GMP levels are associated with increased matrix production and biofilm structure formation, while low c-di-GMP levels are associated with planktonic growth and/or biofilm dispersion. The concentration of this dinucleotide is in turn controlled by various signal transduction pathways in response to multiple environmental cues (Krasteva and Sondermann, 2017; Randall et al., 2022).

c-di-GMP levels are determined by the activities of diguanylate cyclases (DGCs), which synthesize c-di-GMP from GTP, and/or phosphodiesterases (PDEs), which degrade c-di-GMP to produce pGpG. These enzymes bear conserved domains named GGDEF for the cyclases and EAL or HD-GYP for the hydrolases (Krasteva and Sondermann, 2017; Commichau et al., 2006); these domains are often found in tandem as hybrid GGDEF-EAL proteins and joined to multiple transduction domains. Many proteins that synthesize or degrade c-di-GMP contain domains with the ability to sense endogenous or environmental conditions. In addition, the apparent redundancy of these proteins in many of the genomes analyzed so far suggests that bacteria may locally control intracellular c-di-GMP levels (Hengge, 2021).

P. aeruginosa is responsible for the large part of biofilm-mediated nosocomial infections and is the leading cause of death in cystic fibrosis patients (Ha and O'Toole, 2015). Infection sites are heterogeneous microenvironments, and biofilm growth exacerbates the differences in their chemical compositions by leading to the formation of nutrient and oxygen gradients (Jo et al., 2022; Harrison et al., 2021). *P. aeruginosa* exploits diverse physiological strategies that support its survival under hypoxic or anaerobic conditions, including fermentation of environmental arginine (Scribani Rossi et al., 2022), denitrification (Giardina et al., 2011), and reduction of endogenously produced redox-active compounds called phenazines. These compounds move electrons from the deepest layer of biofilm to the surface, where electrons can be delivered to oxygen (Pierson and Pierson, 2010). When limitation for electron acceptors occurs, the accumulation of reducing power stimulates secretion of extracellular matrix. In colony biofilm, the accumulation of matrix leads to an increase of surface area-to-volume ratio (wrinkling) and thereby oxygen exposure for resident cells (Dietrich et al., 2013).

RmcA is a multidomain membrane c-di-GMP PDE that in *P. aeruginosa* integrates signals related to anaerobic metabolism and biofilm physiology (Mantoni et al., 2018; Okegbe et al., 2017; Paiardini et al., 2018). RmcA bears an N-terminal periplasmic binding domain showing a "Venus Fly Trap" fold (VFT) that can recognize arginine. Indeed, *P. aeruginosa* Δ*rmcA* mutants have been shown to accumulate c-di-GMP when arginine is the sole carbon source (Paiardini et al., 2018) and to overproduce matrix even in unfavorable, nutrient-limiting conditions (Katharios-Lanwermeyer et al., 2021). The VFT domain is followed by a transmembrane helix, 4 PAS domains, a GGDEF and an EAL domain (Fig. 1A), which functions as a GTP-dependent PDE (Mantoni et al., 2018). In addition to its role in maintenance of biofilms formed in liquid (Katharios-Lanwermeyer et al., 2021), RmcA has also been shown

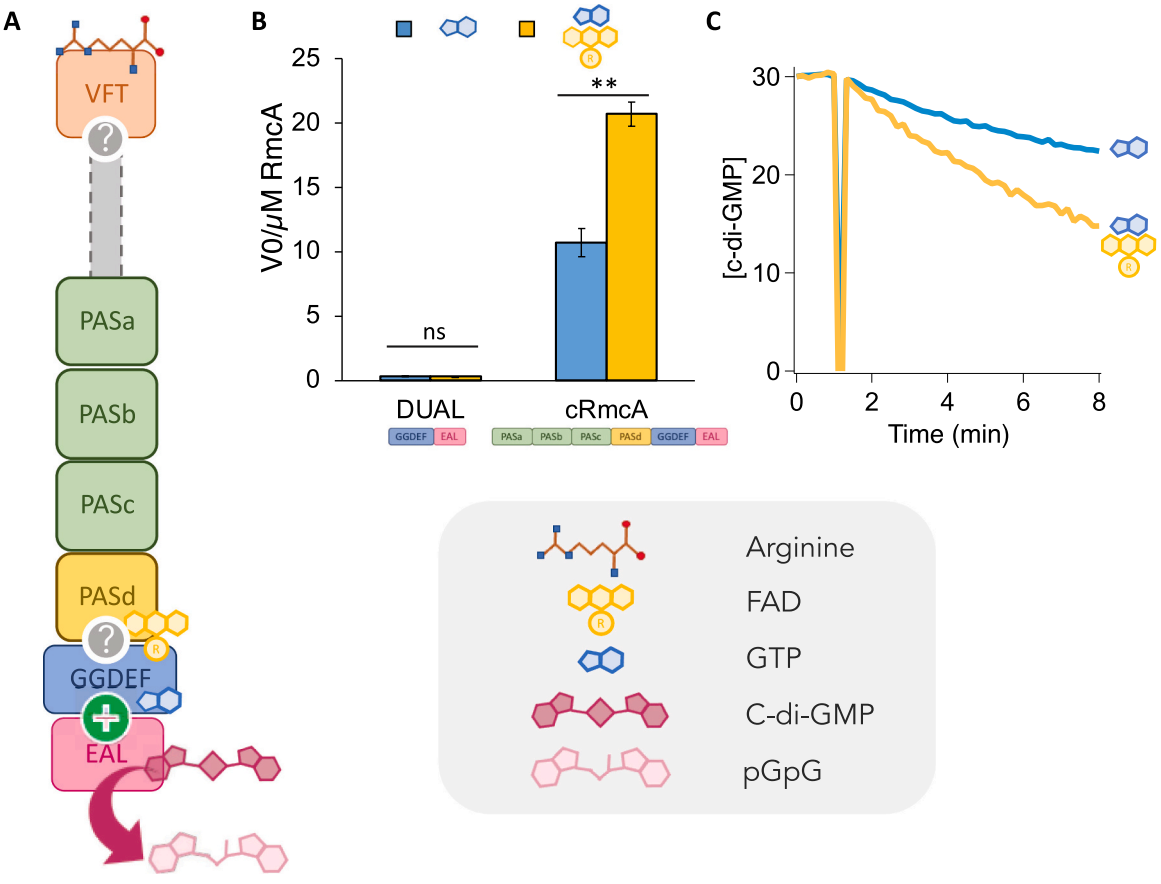

Fig. 1. cRmcA domain organization and PDE kinetics. (A) Domain organization of RmcA, reporting the name's abbreviation of each domain; the ligands/substrate and their target domain are also reported according to the legend boxed in grey. GTP promotes PDE activity ("+" symbol in the Figure, according to (Mantoni et al., 2018). FAD and arginine are known to be recognized by a PAS and the VFT domains, respectively (Okegbe et al., 2017; Paiardini et al., 2018); question marks indicate the lack of mechanistic details related to effect of these ligands on catalysis. (B) Initial velocity v_0/μM enzyme obtained at 30 μM c-di-GMP with DUAL or cRmcA in the presence of 100 μM GTP ± 50 μM FAD. Kinetics were collected following the CD spectroscopic signal of c-di-GMP according to (Stelitano et al., 2013). Data are the mean of at least four experiments ± SD. DUAL samples are not significant different; cRmcA samples are significantly different, * *P < 0.0001. (C) Sample time course of cRmcA kinetics run as described in (B).

to contribute to wild-type biofilm development in colony morphology assays, in which biofilms are grown on agar-solidified media in air or under a controlled atmosphere. In this assay, c-di-GMP levels correlate with matrix production and the onset of wrinkle structure formation. Based on the observation that the protein inhibited biofilm wrinkling in a phenazine-dependent manner, it was given the name "RmcA" for Redox modulator of c-di-GMP (Okegbe et al., 2017). In addition, RmcA has been recently shown to contribute to the inhibitory effect of light on biofilm structure formation (Kahl et al., 2020; Uruén et al., 2021). Mutational analyses suggested that the effects of both phenazines and light mainly depend on the fourth PAS domain, which lies adjacent to the GGDEF domain. However, despite the diverse roles played by RmcA in *P. aeruginosa* biofilm physiology, little information is available regarding the molecular details that link its sensory capabilities to c-di-GMP hydrolysis. In this paper, we present a biochemical analysis of the cytoplasmic portion of RmcA, showing the pivotal role of the C-terminal PAS domain (PASd) in controlling catalysis in response to redox state.

2. Results

2.1. Isolation of the cytoplasmic portion of P. aeruginosa RmcA (cRmcA): N-terminal boundaries and purification

We determined the boundaries of the cytoplasmic portion of the multidomain RmcA protein (Fig. 1A) by performing protein domain analysis and transmembrane helix prediction on the whole sequence of RmcA. The cytoplasmic region, encompassing residues 309–1245, comprises four PAS domains, one GGDEF domain and one EAL domain. We refer to the four PAS domains as PASa-d, with PASa being the most N-terminal and PASd being the most C-terminal domain (upstream the GGDEF domain). Sequence analysis of PASd showed similarity to LOV domains, a family of domains within the PAS "clan" (Almblad et al., 2021) that bind flavin cofactors. LOV domains from diverse bacteria have been studied for their role in conferring light sensitivity in regulatory proteins (Shcherbakova et al., 2015). We thus hypothesized that the PASd domain of RmcA could bind FAD, although it differs from canonical LOV domains in that it lacks a conserved cysteine that contributes to its light-sensing function (Almblad et al., 2021).

The construct containing residues 309–1245, named cRmcA, was heterologously expressed in *E. coli* and purified at the homogeneity (Fig. S1AB). "As purified" cRmcA protein contains a flavin species, likely FAD (Fig. S1C), with a content of ~0.2 equivalents per mole of protein; bacterial growth in the presence of 2 μg/ml riboflavin in the medium does not improve the FAD content (Fig. S1C). This feature agrees with previous observations on a shorter RmcA construct (residues 320–1232, hereinafter cRmcA short), which displayed a UV-Vis spectrum consistent with the presence of FAD, a modest PDE activity and no DGC activity (Okegbe et al., 2017).

2.2. Nucleotides control cRmcA catalysis

cRmcA is a GTP-dependent PDE (Fig. 1B), with a k_{obs}= 10.2 ± 1.2 min^{-1} μM^{-1} at 30 μM c-di-GMP; a minimal DGC activity with the sole GTP was also observed, although it is ~140 folds slower (Fig. S2A).

The GTP-dependent PDE activity is ~31-fold higher than that of the previously characterized GGDEF-EAL construct (referred to as DUAL, Fig. 1A, yielding a k_{obs}=0.33 ± 0.3 min^{-1} μM^{-1} at 30 μM c-di-GMP, (Mantoni et al., 2018).

Pre-incubation of cRmcA with excess FAD positively affects catalysis (k_{obs}=20.4 ± 0.9 min^{-1} μM^{-1}) (Figure 1BC). cRmcA consumes exogenous c-di-GMP over the time and no extra-c-di-GMP accumulation/consumption is observed in the prolonged kinetics, suggesting that no significant GTP consumption occurs also in the presence of FAD (Fig. S2B).

As reported in Fig. 1B, DUAL PDE activity is insensitive to FAD, in agreement with the hypothesis that FAD binding involves the PAS moiety rather than the GGDEF-EAL tandem domain. Accordingly, the binding of the GTP analogue MANT-GTP to cRmcA, which can bind to the GGDEF domain in DUAL, is not affected by excess FAD, further confirming that the two nucleotides do not compete for the same binding site (Fig. S2C).

Given the improved catalytic efficiency of cRmcA as compared to the other constructs of the cytoplasmic portion characterized so far (Fig. S2D, Table I), only cRmcA was further characterized in this study (Table 1).

2.3. Nucleotides control cRmcA oligomerization

We have previously shown by means of Dynamic Light Scattering (DLS) analysis that DUAL undergoes a transition from an "OFF" to an "ON" conformation upon GTP binding (Mantoni et al., 2018). Briefly, GTP binding to the GGDEF domain unlocks the EAL one, which can form the faced EAL-EAL dimer upon c-di-GMP binding to enter catalysis (a cartoon re-calling the EAL activation model is shown in Fig. S3A, according to (Mantoni et al., 2018). On the other hand, DLS analysis on cRmcA indicates that, while GTP does not change the dispersion of cRmcA, the increase in FAD concentration leads to a main population better defined and less heterogenous and the formation of an ever-increasing oligomer population (data not shown). Given the predicted no-globular shape of the protein (Fig. S3B) and the well-known motility of the single domains over the other (Mantoni et al., 2018), we are aware of the limits of DLS in assigning a mass to the species. Therefore, we analyzed the FAD-mediated oligomerization process by means of analytical ultracentrifugation sedimentation velocity (AUC-SV) that allows the simultaneous separation of each oligomer in control range of concentration using their characteristic size, and mass.

As depicted in Fig. 2A, AUC-SV analysis of "as purified" cRmcA reveals the presence of 3 species. Using the fitted frictional ratio, hereinafter f/f_0, (Fig. S4), the sedimentation values were associated with monomers and dimers with different shape. The following species were detected: i) two monomeric species with different sedimentation coefficients, one more globular (7.4 S; f/f_0 =1.10, hereinafter compact form) and, to a lesser extent, one more elongated (5.5 S; f/f_0 =1.45, hereinafter relaxed form), and ii) one relaxed dimeric species with a sedimentation coefficient of 9.1 S and a f/f_0 = 1.4. A protein concentration-dependent equilibrium takes place, involving the compact monomer and the relaxed dimer, while the relaxed monomer amount does not vary with concentration and represent less than 8% of the sample (Fig. 2).

Excess nucleotides dramatically affect the equilibrium between different species and the overall oligomerization state of the "as purified" cRmcA (Fig. 2B). FAD addition promotes the formation of the compact monomer, which is in equilibrium with a newly formed compact dimer (sedimentation coefficient of 11.1 S and f/f_0 =1.15). The relative amount of each species accumulated under different cRmcA concentration was used to estimate an apparent dimerization K_D of 7 μM with an estimated molar ratio of one FAD per cRmcA. Under these conditions, the relaxed monomer is present at trace levels (Fig. 2B).

Table 1
Kinetic parameters of PDE activity (pH 8.0, 25 °C) for RmcA constructs.

PROTEIN	Region	GTP	FAD	K_M (μM)	k_{cat} (min^{-1})	k_{cat}/K_M (μM^{-1} min^{-1})
cRmcA	309–1245	✓	✓	3.2 ± 0.6	24.9 ± 1.1	9.18
cRmcA short	320–1232	✓	✓	2.1 ± 0.6	5.9 ± 0.3	2.8
DUAL	809–1245	✓	-	2.5 ± 0.5(Mantoni et al., 2018)	0.35 ± 0.1(Mantoni et al., 2018)	0.14

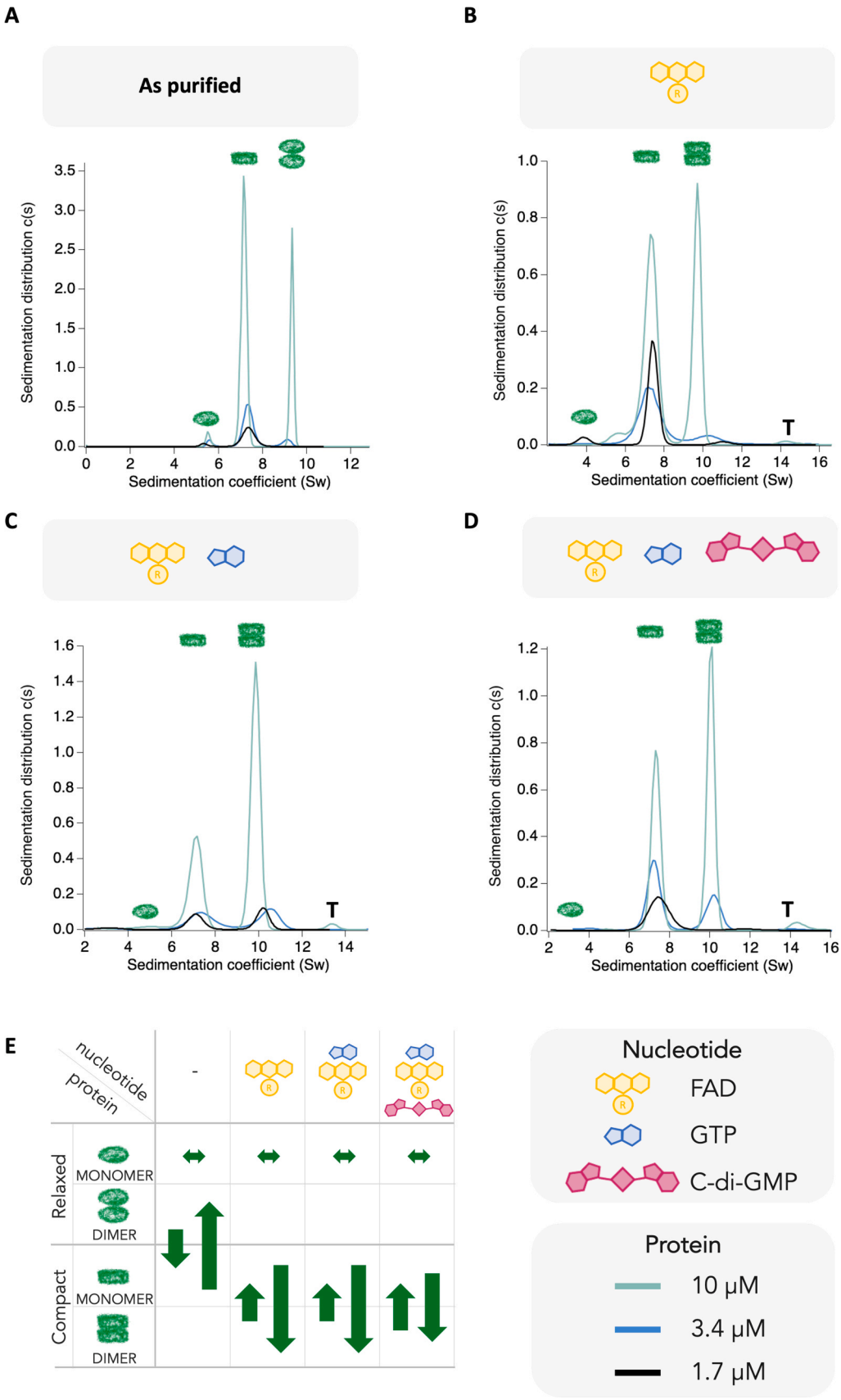

(caption on next page)

Fig. 2. Effect of nucleotides on cRmcA oligomerization. (A-D) Sedimentation coefficient distribution obtained by analytical ultracentrifugation sedimentation velocity (AUC-SV) of cRmcA. Data were obtained at 3 different protein concentrations: 1.7 μM (black traces), 3.4 μM (light blue traces) and ~10 μM (green traces; precisely, 10.1 μM for the "as purified" sample (A) and 9.2 μM for samples with excess nucleotides (B-D)). Samples were assayed "as purified" (A), with excess FAD (B), with excess FAD and GTP (C) or with excess FAD, GTP, c-di-GMP (D). Nucleotide concentration was 50 μM for FAD, 100 μM for GTP and 30 μM for c-di-GMP. The experiment was done in 10 mM Hepes, 300 mM NaCl pH 7.5 buffer supplemented with 2.5 mM $CaCl_2$. (E) Possible equilibrium scheme established upon nucleotide (s) addition to cRmcA, as observed by AUC-SV. In the "as purified" sample, the amount of relaxed monomer does not depend on protein concentration, so this species is not included in the equilibrium. Arrows indicate equilibria between species and are based on the concentration-dependence observed in the AUC-SV measurements. Rows contain the protein species and columns contain the nucleotide added in excess, in each experiment. Boxed in grey i) the legend of the symbols used for the excess nucleotides present in the protein solution; ii) the color code used for the different protein concentrations.

This trend is augmented by the co-presence of GTP and FAD (Fig. 2C), which results in a shift towards the compact dimer species in a protein concentration-dependent fashion with an estimated dimerization constant of ~ 3 μM. Given that GTP and FAD largely increase the catalytic PDE activity of cRmcA, it is likely that the compact dimer is the catalytically competent species under these experimental conditions.

The effect of c-di-GMP on the oligomerization properties of the GTP/FAD-containing cRmcA was assayed, by taking advantage of $CaCl_2$, instead of Manganese, which allows cRmcA to bind nucleotides without entering turnover. As depicted in Fig. 2D, the main species detected are again the compact monomer and the compact dimer, with a slight increase of the monomeric species as compared to results shown in Fig. 2B and C.

It is worth mentioning that, regardless of the nature of the nucleotide (s) added, a tetrameric species is also observed ("T" in Fig. 2), although it represents less than 1–3% of the overall species; it is not excluded this oligomeric state could be populated in the full-length protein. Based on our compiled AUC-SV data, we propose a scheme of RmcA's conformational equilibria, and the associated effects of nucleotide addition, as depicted in Fig. 2E.

These data confirm that the catalytically competent conformation is the compact state and that an equilibrium between the two oligomerization states may take place during turnover (upon substrate binding or product release for example).

To shed light on the FAD:cRmcA complex, we performed native mass spectrometry (nMS) analysis (Fiorentino et al., 2023; Fiorentino et al., 2021). "As purified" cRmcA (1 μM) was buffer exchanged into nMS-compatible ammonium acetate (200 mM) buffer; this protein was shown to exists mostly as a monomer (χdimer = 0.28 ± 0.01) (Fig. 3A). 10-fold excess of FAD (10 μM) clearly induced dimerization, as the mole fraction of the dimer increased almost by 3-fold (Fig. 3A-C). Notably, cRmcA molecular masses increased of ~780 Da for monomeric cRmcA and ~1510 Da for dimeric cRmcA, which is consistent with binding of 1 and 2 FAD molecules, respectively (Supplemental Table S5). These results are in agreement with the FAD/cRmcA estimated by AUC. Overall, these findings suggest that cRmcA interacts with FAD in a 1:1 ratio in both its monomeric and dimeric forms (per monomer). The FAD-dependent oligomerization does not limit the accumulation of the catalytically competent species under steady state and pseudo-first order conditions since the time course and the turnover depend linearly on enzyme concentration (Fig. S3C).

2.4. FAD controls the PDE activity of cRmcA in a redox-dependent fashion

In addition to their roles as co-substrates in metabolic reactions, flavins can also regulate protein function in a redox-dependent manner (Becker et al., 2011). In flavin-containing redox sensors, protein function is controlled by the redox state of the cofactor (Orr et al., 2015). Given the allosteric effect of FAD in RmcA, we probed whether the redox state of the flavin moiety may control RmcA catalysis differently. We carried out kinetic assays under hypoxic conditions with N_2-flushed solutions in sealed vials and cuvettes; under these conditions $FADH_2$ can be populated in the presence of reductant/O_2 scavenger in slight excess (500 μM sodium dithionite; CD spectra of c-di-GMP with excess dithionite, used as reference, are depicted in Fig. S5A). As control, the reaction with sole GTP was run under the same experimental conditions (Fig. S5B).

We found that, in contrast to oxidized FAD (Fig. 4A, yellow trace, obtained after N_2-flushed in sealed cuvette), reduced FAD ($FADH_2$) failed to activate the protein (Fig. 4A, grey trace). This evidence suggests that FAD may exert a fine-tuning of the PDE activity of cRmcA in response to the cellular redox state.

Previous work phenotypically linked RmcA to phenazines, the electron shuttles used by *P. aeruginosa* to cope with anaerobiosis and found that the cytoplasmic portion of RmcA bound to these molecules in vitro (Okegbe et al., 2017). We observed that reduced pyocyanin per se was not able to affect PDE cRmcA activity (Fig. S5B), suggesting that the effect of phenazines observed on biofilm could be mediated by FAD/-$FADH_2$ ratio in the cell. In *P. aeruginosa,* phenazines are known to act as respiratory electron acceptors under anaerobic conditions, contributing to maintenance of proper NADH/NAD^+ and $FADH_2$/FAD ratios within the cell, when O_2 is limiting (Jo et al., 2017; Okegbe et al., 2017; Pierson and Pierson, 2010). Under this view, the $FADH_2$/FAD switch observed in cRmcA may represent the mechanistic link between phenazine redox state and RmcA activity (Okegbe et al., 2017).

2.5. PASd is an FAD-dependent LOV-like domain

A significant number of proteins bearing flavin-dependent redox switches contain PAS domains (Becker et al., 2011). A subset of these PAS domains (i.e the LOV domain) contains a conserved cysteine residue that is required for sensory function (Commichau et al., 2006).

According to domain composition analysis of RmcA, a domain with high similarity to other well-studied LOV domains is present in the region encompassing residues 681–801, before the downstream GGDEF-EAL DUAL motif (Fig. 1). However, this PASd domain lacks the conserved cysteine residue that is present in canonical LOV domains. The core structure of the PASd domain is composed of a five-stranded antiparallel β-sheet, surrounded by three short α-helices and several solvent-exposed loops (Fig. 4B). This topological arrangement generates a barrel-shaped module that forms a symmetric dimer with the other PASd domain of the adjacent subunit and hosts a hydrophobic pocket in the interior of the PASd domain.

A large number of hydrophobic side chains, such as Met697, Phe712, Pro728, Leu731, Met744, Trp745, Ile758, Leu772, Ile774, Phe787 and Phe791, form a cavity that could bind small organic ligands. Thanks to the high similarity with other FAD-containing LOV domains, it was therefore possible to model the FAD cofactor inside the deep hydrophobic cleft of the RmcA PASd domain (Fig. 4B).

Asn760 is highly conserved in FAD-binding LOV domains, and it has been shown that mutation of the homologous residue in AxDGC2, a redox-sensing DGC found in *Komagataeibacter xylinus*, abolished binding of FAD (Qi et al., 2009). As shown in other LOV domains, the prompt reorganization of an internal hydrogen-bonding network in response to the FAD cofactor redox state could be pivotal for signal sensing and transduction. In our model, Asn760 and Glu770 are predicted to rearrange their sidechain conformations to optimize this hydrogen-bond network with $FADH_2$ (Fig. 4C). In turn, according to our model, the transmission of this signal across the adjacent β-sheet is made possible by Tyr768. Finally, the alteration of the β-sheet surface affects the conformation of a downstream helix that lies adjacent to the PASd

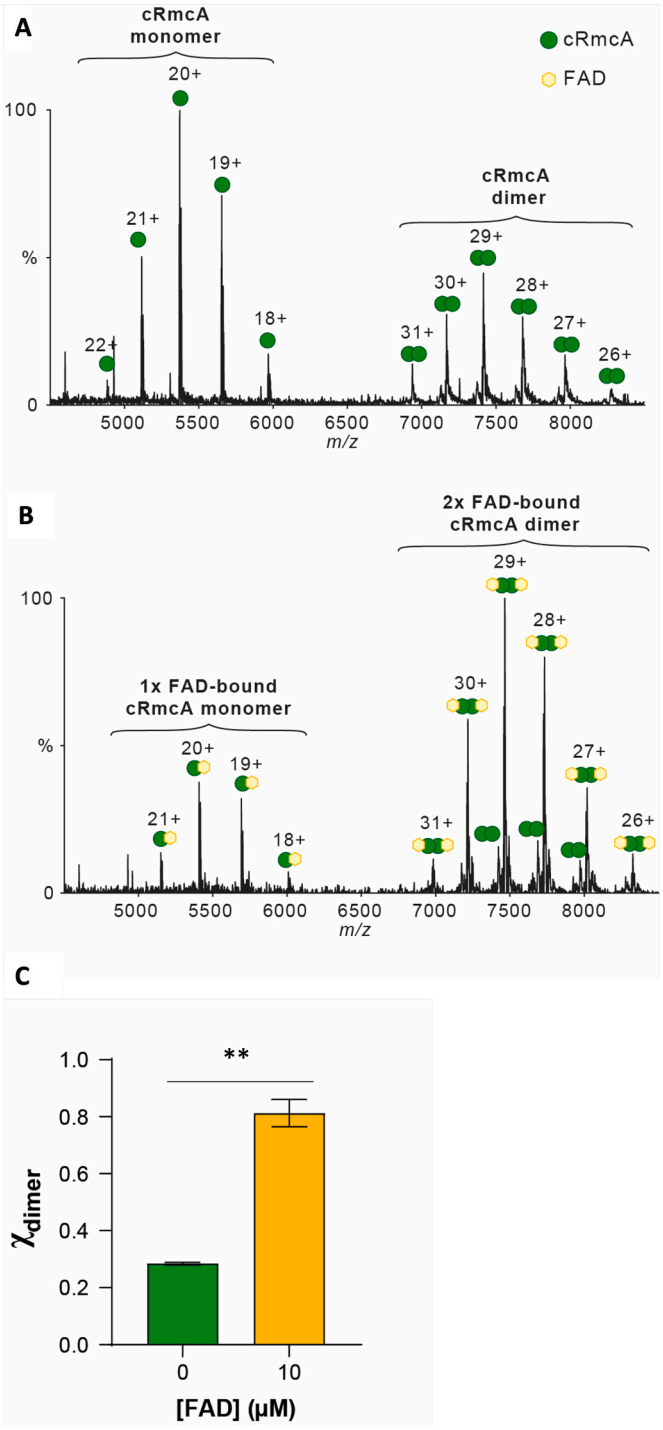

Fig. 3. Native MS of cRmcA (1 μM) in its apo-form (A) or in the presence of FAD (10 μM) (B) illustrating the FAD-induced dimerization. For each assigned complex, the charge state for every peak is shown, with the sign denoting data collection in positive mode. (C) Bar chart of cRmcA dimer mole fraction (χ_{dimer}) as a function of FAD concentration. Data are the mean of at three independent experiments (n = 3) ± SD. * * P < 0.0001.

domain core and bridges the PASd domain with the GGDEF-EAL C-terminal domains. Indeed, the PASd domain of RmcA is flanked by a short sequence (residues 794–808) connecting the PASd domain to the GGDEF domain and predicted to fold as an α-helical segment. This region is homologous to the "S-helix" of *P. aeruginosa* cRbdA, which is known to play a key role in holding the EAL domains locked in place (Liu et al., 2018). Notably, in RmcA, Tyr799 of this region points towards the FAD binding site of the upstream PASd domain and it could act as a "hinge" between PASd and GGDEF-EAL domains.

2.6. Mechanism of FAD-mediated redox sensing

Both the structural predictions presented in this study and previously published data (Okegbe et al., 2017) suggest that the PASd domain binds to FAD via stacking of the conserved Trp745 with the adenine moiety of FAD. Mutation of Trp745 to Ala led to an earlier onset of colony biofilm wrinkling, consistent with the hypothesis that PASd-dependent redox sensing stimulates RmcA PDE activity and inhibits matrix production in vivo (Okegbe et al., 2017). The W745A mutant of cRmcA lacks the typical UV-Vis spectrum of the FAD adduct (Fig. S6), but nevertheless it shows a wildtype-like PDE activity when FAD is provided in excess (50 μM) (Fig. S6 and Fig. 5). Differently from the wildtype protein, W745A needs larger FAD excess to reach the maximal PDE velocity (Fig. S6), thus suggesting that the apparent affinity for FAD is lowered by mutation and confirming the involvement of the PASd Trp745 residue in stabilizing the FAD:cRmcA interaction. Despite the mutation, W745A is still able to respond to the variation of the redox state of FAD (in excess), showing a lowered rate of c-di-GMP hydrolysis in the presence of $FADH_2$ (Fig. 5B). Therefore, although this mutation is expected to affect the region involved in adenine stabilization, it does not contribute to our understanding of the mechanism of allosteric control exerted by FAD/-$FADH_2$ over the GGDEF-EAL motif.

The conserved Asn760 is predicted to contact FAD via its isoalloxazine ring and possibly contribute to sensing the different redox states of FAD (Fig. 4B). The Asn760 to Ala mutation leads to a protein lacking FAD spectral signal (also after in vitro reconstitution, Fig. S6A), suggesting that the affinity for this nucleotide is dramatically affected. Interestingly, this protein showed a constitutively active PDE activity, insensitive to the presence of excess FAD or $FADH_2$ (Figure 5BC and Fig. S6B). This result indicates that, beyond its role as FAD interactor, Asn760 participates in controlling the conformational transition $Low_{PDE} \rightarrow High_{PDE}$ by sensing the FAD cofactor (regardless of the redox state). The substitution of Asn760 with Ala hampers the interaction with FAD and, more importantly, allows cRmcA to populate the $High_{PDE}$ conformation. The constitutively $High_{PDE}$-like state of the N760A mutant is confirmed in vivo, as biofilms formed by the RmcA N760A mutant show a severe delay in the onset of wrinkling when compared to the WT (Fig. 5). This delay is recapitulated in the phenazine-null mutant background, indicating that the effect of this mutation arises independently of the cellular redox state or the presence of phenazines (Fig. S7). The fact that the N760A mutation not only perturbs the interaction with FAD but forces the protein to adopt an "ON" conformation indicates that this region is relevant for transduction (conformationally over the GGDEF-EAL motif) of the signal mediated by the FAD-redox state, in agreement with the structural predictions.

2.7. Mechanism of redox-dependent allosteric control of cRmcA PDE activity

As mentioned above, Glu770 is a good candidate as an interactor of Asn760 and as a transducer of the redox signal. Mutation of Glu770 into Ala (E770A) leads to a FAD-containing, "as purified" protein with a FAD-dependance close to that of wildtype but with a ~ 25% lower turnover (Fig. S6). The most striking difference is observed upon FAD reduction, where the E770A mutant is unable to respond to $FADH_2$ as indicated by the fact that the PDE k_{obs} is unaffected in this condition (Fig. 6). Therefore, while the positive effect on kinetics due to FAD (and mediated by Asn760) is still present in the E770A mutant (Fig. 6A, yellow bar), the subsequent redox-dependent transduction is abolished by the mutation, suggesting that Glu770 is involved in the conformational change required to populate the Low_{PDE} state upon FAD reduction.

While Asn760 conservation is an established trait of the FAD-dependent LOV domains, Glu770 is conserved to a lesser extent; a

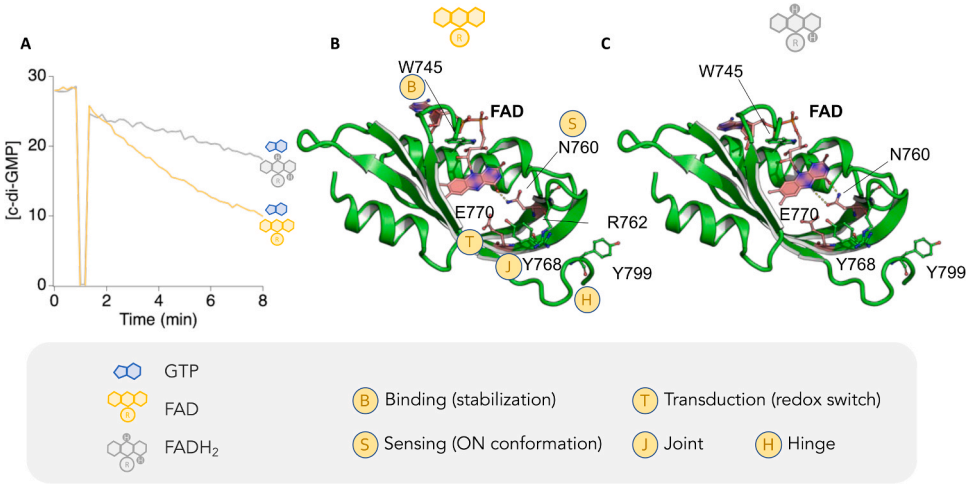

Fig. 4. Effect of FAD reduction state on cRmcA activity. (A) PDE time course of cRmcA under hypoxic conditions in the presence of 100 μM GTP and 50 μM FAD, added in its oxidized form (yellow line) or reduced form. $FADH_2$ was prepared by treating with 500 μM sodium dithionite (grey line). (BC) Structural model of the PASd domain of RmcA (residues 681–801) with oxidized (B) and reduced (C) FAD bound. The different network of polar contacts within the FAD binding cleft upon cofactor oxidization/reduction is depicted, with key residues. These residues are labeled with a letter according to the proposed role in FAD/$FADH_2$ redox-swtich; in particular, (B) for binding FAD, (S) for sensing redox state, (T) for signal transduction, (J) for Joint and (H) for Hinge.

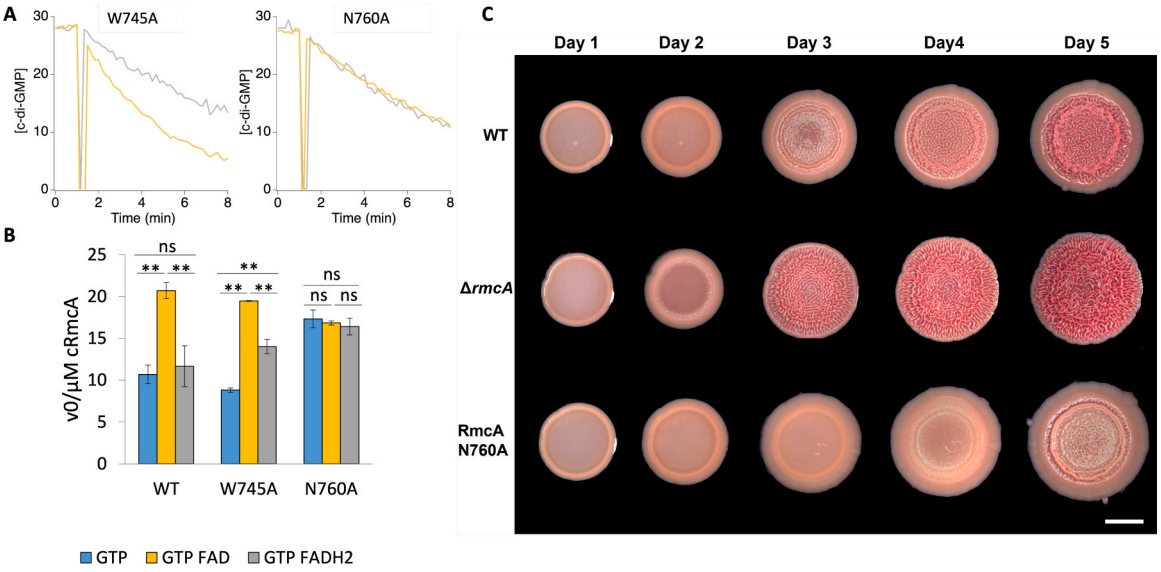

Fig. 5. FAD-dependence of PDE kinetics in FAD-interacting cRmcA mutants. (A) PDE time course of cRmcA mutants, indicated in each graph, under hypoxic conditions in the presence of 100 μM GTP and 50 μM FAD, oxidized (yellow line) or reduced anaerobically with 500 μM sodium dithionite (blue line). (B) Initial velocity v_0/μM enzyme obtained at 30 μM c-di-GMP with cRmcA variants indicated in the X-axis, in the presence of 100 μM GTP (blue bars), 50 μM FAD (yellow bars) and $FADH_2$ (grey bars). Data are the mean of at least four experiments ± SD. Grey bars are significantly different from the corresponding yellow ones (P value <0.001) with the exception of the N760A mutant, where no significant differences were observed. (C) Representative images of *P. aeruginosa* PA14 WT, ΔrmcA, and the RmcA N760A mutant at the indicated time points during growth in the colony biofilm morphology assay. (Scale bar, 1 cm). Images were taken daily using a Keyence VHX-1000 microscope.

serine residue was found to be mainly present in other RmcA among *Pseudomonads* (Fig. S8). Mutation of Glu770 to serine indeed leads to a behavior very similar to the E770A mutant (Fig. S9A), thus indicating that the capability to respond to different redox states of FAD could be evolutionarily lost, depending on the biological background in which the PASd domain functions. Accordingly, cRmcA from *P. putida*, whose sequence bears the serine residue in the homologous position, is a FAD-dependent PDE unable to respond to the redox state of the flavin moiety (Fig. S8C).

Structural modeling suggests that the two conformational states (i.e. FAD or $FADH_2$ bound) of the PASd domain are both sensed by Tyr768, whose predicted role is to transmit this signal to the downstream Tyr799 (see below) and GGDEF/EAL domains of RmcA, acting like a bridge between the sensing core and the effector units. Indeed, its substitution into alanine dramatically affected the overall catalytic profile of cRmcA in terms of observed rate, although it still responds to FAD in a redox-dependent fashion (Fig. 6A).

A summary of the effect of mutations on the transduction cascade events is provided in Fig. 6B: i) protein conformational change upon FAD binding (N760A), ii) redox-dependent transduction (E770A), iii) conformational transmission of the integrated information (Y768A).

Downstream of the PASd domain, all the sensory information must be communicated to the catalytic moiety. The EAL domains are likely held as a monomeric entity by the upstream domain(s) to sustain the

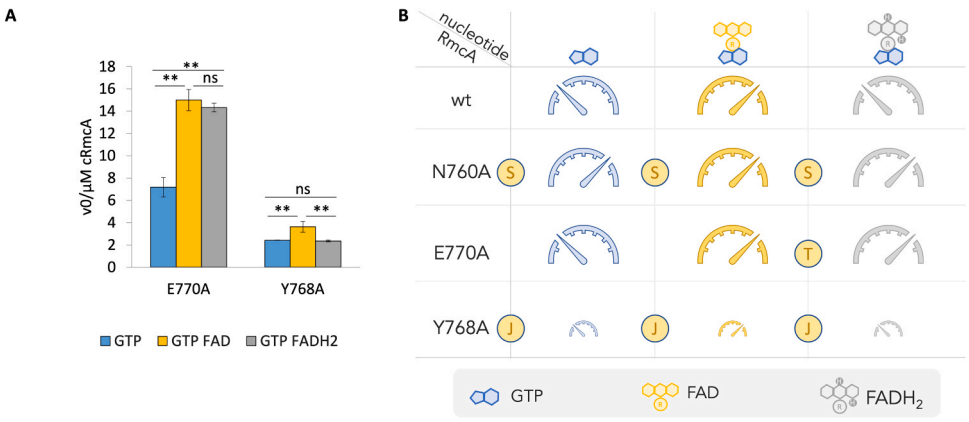

Fig. 6. FAD-dependence of PDE kinetics in different cRmcA mutants. (A) Initial velocity v_0/µM enzyme obtained at 30 µM c-di-GMP with cRmcA variants indicated in the X-axis, in the presence of 100 µM GTP (blue bars), 50 µM FAD (yellow bars) and $FADH_2$ (grey bars). Data are the mean of at least four experiments ± SD. In E770A, grey bar is not significantly different from the corresponding yellow one (P value > 0.01); in Y768A, grey bar is significantly different from the corresponding yellow one (P value < 0.001). (B) A cartoon summarizing the kinetics profile of wt cRmcA and the different mutants relevant to the redox-dependent tuning of PDE activity. The effect on the PDE activity tuning is depicted as a tachometer: Low_{PDE} or $High_{PDE}$ are depicted with the needle on the left or on the right, respectively. Small tachometer cartoons for Y768A mutant refers to an overall reduced turnover as compared to the wt. The label with circled letters indicates the role identified for each key residue in FAD/$FADH_2$ redox-switch, according to the corresponding mutant kinetics behavior. In particular, (S) for sensing redox state, (T) for signal transduction, (J) for Joint.

OFF conformation (Mantoni et al., 2018); their release establishes the catalytically competent species through the conserved S-helix. Our data suggest that Tyr799 may function as a hinge that transfers the redox switch message to the GGDEF-EAL DUAL moiety. In agreement with bioinformatics analysis, substitution of this residue with Ala strongly affects cRmcA in terms of i) kinetics, which are dramatically decreased, comparable to those of the sole DUAL or to the GTP-free cRmcA (Fig. S9B); ii) FAD-interaction, which is partly restored by in vitro reconstitution (Fig. S9C); and iii) FAD-dependence of PDE turnover, which is only GTP-dependent (Fig. S9B), thus uncoupling the PASd FAD interaction and the allosteric control of the DUAL portion.

3. Discussion

Biofilms are characterized by the stratification of metabolic signatures, arising from gradients of nutrients and oxygen. Cells on the periphery of this multicellular structure consume oxygen faster than it can diffuse into the deeper layers; this phenomenon leads to a hypoxic or even anoxic environment deep within the biofilm. Biofilms growing on nutrient sources are characterized by excess intracellular electron donors and shortage of electron acceptors, such as oxygen, at the biofilm base (Jo et al., 2022). Reduced oxygen levels contribute to decreased sensitivity to traditionally recommended antibiotics (Gupta et al., 2016); in particular, a decrease in the membrane potential, which can arise from the redox imbalance experienced under anaerobic/hypoxic conditions within biofilm, is reported to be a crucial factor in bacterial tolerance to some antibiotics (Uruén et al., 2021; Benarroch and Asally, 2020). The development of this redox imbalance can be counteracted by increased matrix production, which stimulates the formation of vertical structures (named wrinkles) that increase the surface area-to-volume ratio macrocolony biofilms (Commichau et al., 2006), allowing a greater proportion of resident cells to have access to oxygen.

Aside from structure formation, bacteria may channel electrons belonging to central metabolism to environmental oxidants at a distance, through a variety of strategies named "extracellular electron transfer" (EET) (Saunders et al., 2020; Yalcin and Malvankar, 2020).

P. aeruginosa mitigates redox imbalance under oxygen-limited conditions by transferring electrons to the endogenously produced phenazines. Phenazines are diffusible, redox-active small molecules that can accept electrons from cells in hypoxic biofilm subzones and facilitate electron transfer to oxidants (such as oxygen) that are only available at a distance (Fig. 7, left panel). The results of genetic studies indicate that RmcA acts as a link between redox or phenazine sensing and the regulation of biofilm structure formation (Okegbe et al., 2017), but the underlying molecular mechanism has not been elucidated.

In this paper, we report a biochemical study of the cytoplasmic portion of RmcA (cRmcA). A truncated version of RmcA, containing the GGDEF and EAL domains, was previously found to be a GTP-dependent c-di-GMP phosphodiesterase (Mantoni et al., 2018). Here we found that cRmcA activity is further controlled by the LOV-like domain PASd, located immediately upstream the GGDEF-EAL catalytic moiety. Our results show that this domain finely tunes catalysis through the FAD cofactor and that this control is tuned in a redox-dependent manner, with higher PDE activity correlating with the presence of oxidized FAD. The reducing power of the cell (Heikal et al., 2010), represented by FAD/$FADH_2$ and NAD/NADH ratios, correlates with phenazine populations (i.e., oxidized vs reduced). The phenotypic consequence of this sensing activity is that RmcA efficiently degrades c-di-GMP when oxidized phenazines accumulate and/or when the redox state of the cell is relatively oxidized; this increased c-di-GMP consumption leads to decreased matrix production, thereby inhibiting biofilm structure formation. Such a regulatory relationship is consistent with a model in which phenazine metabolism and biofilm wrinkling represent alternative strategies for coping with oxygen limitation in biofilms; RmcA acts as a transducer that inhibits wrinkling in the presence of phenazines and favors wrinkling when phenazines are not available.

At the molecular level, multiple nucleotides activate or control cRmcA activity in a multilayered fashion. FAD and GTP act via the PASd and the downstream GGDEF domain, respectively, as allosteric regulators. C-di-GMP itself acts as an allokairic ligand (Hilser et al., 2015), since, beyond its binding to the active site, the subsequent turnover sustains over the time the catalytically competent form of the EAL domain as a dimeric entity (Mantoni et al., 2018; Navarro et al., 2011; Rao et al., 2009). For each nucleotide, a different mechanism of control and a distinct role has been proposed. It should be mentioned that in addition to this regulation of the cytoplasmic portion of the protein, a capacity for arginine sensing appears to be conferred by the periplasmic portion (Paiardini et al., 2018) (Fig. 7, blow-up).

Due to its complexity, we have previously proposed and, in this paper, partly demonstrated that RmcA may represent a rheostatic protein (Paiardini et al., 2018). It is now recognized, particularly for transducers, that, in the control of cellular processes, these proteins are

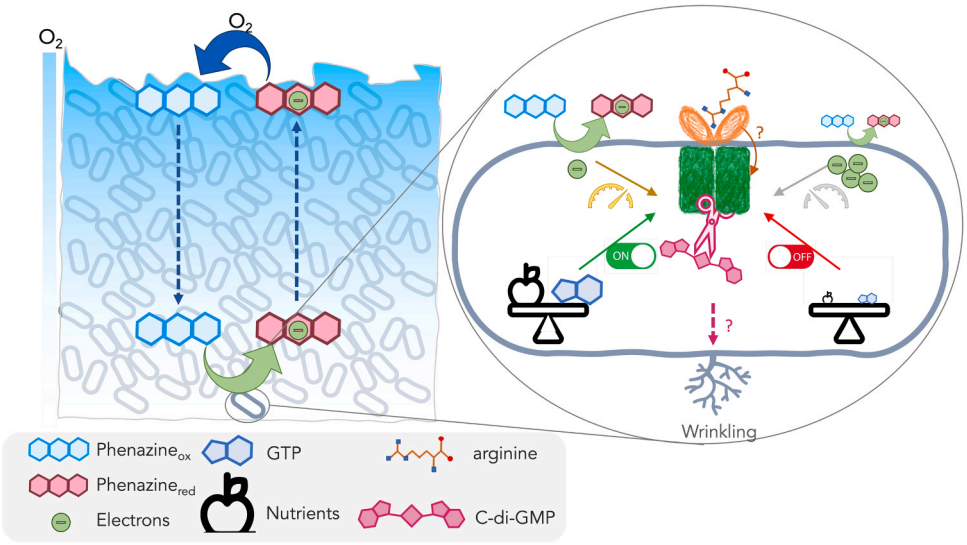

Fig. 7. Possible model linking phenazine cycle and RmcA c-di-GMP hydrolysis. Diagram of the phenazine redox cycle in a biofilm, where the oxygen gradient within the biofilm matrix is represented as light blue shades and cells as gray rods. A legend of symbols used to depict phenazines (reduced and oxidized), electrons, GTP, nutrients and c-di-GMP is shown at the bottom. The inset depicts a model showing proposed relationships between extra- and intracellular conditions and RmcA function: (i) phenazine availability shifts the cellular redox state to be oxidizing, stimulating RmcA activity via the PASd domain, as described in this study; (ii) nutrient availability correlates with levels of GTP, which acts as a switch to activate RmcA; and (iii) arginine binds to the periplasmic domain of RmcA and may activate or tune protein activity. RmcA acts as a phosphodiesterase to cleave c-di-GMP, which leads to lower levels of matrix production and inhibits biofilm wrinkling. The scheme represents a possible network of different phenomena and is not a precise picture of the molecular interactions that may be taking place. Protein oligomerization and conformational changes are not depicted.

not always acting simply as "on" or "off" entities (toggle switches). Instead, they can act as rheostats, ensuring multiple levels of modulation leading to distinct and diverse cellular outcomes (Wu et al., 2019; Kawashima et al., 2013).

Fine tunability is often associated with extraordinary protein structural plasticity (Ruggiero et al., 2022), and RmcA is a stunning example of this. The crystal structure of the DUAL dimer revealed two distinct conformations with striking differences with respect to the reciprocal domain orientation between the monomers (Mantoni et al., 2018).

In vivo and in vitro studies with mutant versions of RmcA are also consistent with the notion that this protein's large and flexible structure supports complex interdomain interactions as well as conformational control. For example, deletion of RmcA's N-terminal PAS domain, PASa, leads to a decrease in biofilm matrix production, in contrast to the increased matrix-production phenotypes exhibited by the ΔrmcA mutant or mutants lacking any of the other PAS domains (Okegbe et al., 2017); accordingly, we found that two different N-terminal PASa boundaries, which differs in length by only 11 residues, contribute significantly to the EAL catalytic profile (Table 1). Accordingly, while the redox switch is confirmed by *in cellulo* data, some mechanistic details observed with cRmcA may change with the full-length protein, whose behavior also responds to the membrane environment, the periplasmic signals and potential macromolecular interactors.

We found that binding of oxidized FAD to cRmcA promotes high PDE activity and that turnover slows down (~two-fold) once FAD becomes reduced. The ability to perceive FAD is associated with Asn760, which in turn transmits the information to Glu770. Substitution of Glu770 with Ala uncouples FAD sensing from FAD/$FADH_2$ discrimination. Glu770 is not widely conserved among *Pseudomonads* RmcA orthologues (Fig. S9), as expected for rheostatic residues, which generally account for protein polymorphisms (Meinhardt et al., 2013).

LOV/PAS domains are often found in multiple copies, some of which may serve as scaffolds for protein oligomerization in response to redox signals to the neighboring LOV/PAS domain, as in the case of the NifL regulator from *A. vinelandii* (Little et al., 2012). It is likely that a similar mechanism takes place also in RmcA, upon nucleotide binding; the RmcA LOV-like domain is indeed located downstream 3 further PAS domains, which should respond to the periplasmic signal and could mediate the oligomerization observed in the AUC-SV and DLS analysis of cRmcA.

The PAS-mediated FAD/$FADH_2$ ratio perceiving is a conserved strategy used in bacteria to monitor internal conditions related to electrons balancing. As an example, in the "energytaxis" phenomenon mediated the Aer transducer, the PAS domain controls the oligomerization and the activation of the chemo-transducer, by changing its conformation in response to FAD/$FADH_2$ ratio change (Samanta et al., 2016; Garcia et al., 2016).

RmcA was also found to be involved in maintenance of biofilms grown in liquid cultures, with the deletion mutant showing increased sensitivity to nutrient limitation (Katharios-Lanwermeyer et al., 2021). We have previously reported that the periplasmic portion of RmcA recognizes L-arginine and promotes c-di-GMP consumption when it is the sole carbon source (Paiardini et al., 2018). Future studies will be required to assess whether the periplasmic portion accounts for the nutrient-related phenotype, while the intracellular domains may contribute to biofilm maintenance, when the oxygen gradient and the hypoxic layer are well established.

The global nutritional status is generally controlled by GTP (Lopez et al., 1981), which is one of the allosteric activator of RmcA (and other GGDEF-EAL proteins) (An et al., 2010; Mantoni et al., 2018). Cellular GTP levels should be high enough to saturate the RmcA GGDEF domain (Paiardini et al., 2018), though it is noteworthy that under stressful conditions or nutrient starvation, the GTP pool is significantly depleted (up to 80%) to produce the alarmone 3′,5′-(bis)pyrophosphate (ppGpp) and re-program cellular metabolism (Bittner et al., 2014; Chiaverotti et al., 1981). In cRmcA, GTP sustains catalysis in an "all or nothing" fashion ($10.2 \pm 1.2\ min^{-1}\ \mu M^{-1}$ vs $0.33 \pm 0.3\ min^{-1}\ \mu M^{-1}$ at 30 μM c-di-GMP, respectively), by *de facto* activating the c-di-GMP hydrolysis. It is possible that the EAL domains of RmcA (and other GGDEF-EAL tandem proteins) are switched off when GTP levels are low, and the biosynthetic potential is therefore not optimal; this evidence indicates that the EAL-EAL facing induced upon GTP binding (Mantoni et al., 2018) is necessary to enter and sustain catalysis, regardless of the dimerization of the whole cRmcA induced by FAD.

Therefore, while FAD/$FADH_2$ finely tunes the turnover rate in a redox-dependent fashion (~2 folds activation with the FAD as compared to $FADH_2$, represented as a tachometer in Fig. 6), GTP acts as a real switch of catalytic activity (~31 folds activation, represented as a switch in Fig. 6).

With respect to the cellular redox state, the cytoplasm is generally described as "reducing" due to the prevalence of reduced glutathione, but measurements of the cellular NADH/NAD^+ ratio indicate that the availability of alternate electron acceptors such as phenazines can shift the redox state to become more oxidizing (Dietrich et al., 2013; Price-Whelan et al., 2007). This is likely to affect the FAD/$FADH_2$ ratio and thereby tune RmcA-mediated c-di-GMP consumption.

A compilation of possible mechanisms of RmcA regulation is diagrammed in Fig. 7. Therefore, the differential effects of the two allosteric regulators could be related to their distinct roles in cellular metabolism, or to condition-dependent differences in their availability.

In summary, the results of this study provide insight into the molecular mechanisms enabling RmcA to link redox sensing to PDE activity, and therefore biofilm structure formation, in *P. aeruginosa*. The *P. aeruginosa* genome encodes multiple proteins with the potential to modulate c-di-GMP in a redox-dependent manner (Das et al., 2015), raising the possibility that their activities are integrated to fine-tune the sensitivity of biofilm development to exogenous and endogenous redox states. Redox-sensitive modulation of c-di-GMP levels also occurs in the bacterium *Komagataeibacter xylinus*, where a DGC and a PDE simultaneously function to promote cellulose production in the presence of oxygen. Cellulose production allows *K. xylinus* to form a pellicle biofilm so that it can remain suspended at the interface with air and access oxygen in a standing liquid culture. The animal and plant worlds also contain numerous examples of redox-based control of multicellular development, underscoring that gradient formation and resource limitation are fundamental drivers of biological structure formation. It is now well acknowledged that in the host–microbe microenvironment, bioelectrical factors, including phenazines, extracellular DNA and nanowires, govern the physiological statuses of microbes and influence their interactions with the host. Knowledge gained from mechanistic studies of redox sensing and biofilm development can form the basis for novel electroceutical solutions to the problem of microbial recalcitrance (Sen et al., 2020).

More generally, as we continue to characterize the mechanisms that link redox conditions to the morphogenesis of multicellular systems, we expect to gain further insights into this broad developmental principle in Biology (Jo et al., 2022; Sporer et al., 2017).

4. Experimental procedures

Protein expression and purification: *P. aeruginosa* PAO1 cRmcA (amino acid residues 309 – 1245) was obtained from pet28-HisTag-RmcA (Paiardini et al., 2018) by PCR deletion (Hansson et al., 2008). The cytoplasmic portion of *P. putida* RmcA (residues 309–1248) was obtained as a synthetic construct (Genescript) cloned in Pet28b fused to a C-terminal His-tag. Site-directed mutants and deletion were obtained by PCR of the whole plasmid using Q5 High-Fidelity DNA Polymerase (Biolabs). The PCR was followed by *Dpn*I (Biolabs) digestion, then transformed in *Escherichia coli* Neb 5-alpha competent cells (Biolabs) and mutation was confirmed by DNA sequencing. Mutagenesis and PCR deletion oligonucleotides, plasmids and strains used in this study are reported in Table SI and SII.

The different proteins were overexpressed in the *E. coli* BL21 (DE3) strain. Bacterial cultures were grown at 37 °C in Luria-Bertani (LB) liquid medium with 30 μg/ml Kanamycin (Sigma) until OD_{600}~ 0.8 and then the temperature was reduced to 18 °C for 20 h after addition of 0.1 mM IPTG (isopro- pyl β-D-thiogalactoside; Sigma Merck) (16 °C for *P. putida* cRmcA).

Cells were harvested by centrifugation and bacterial pellets were suspended in lysis buffer (50 mM Hepes pH 7.5, 500 mM NaCl, 5% Glycerol, 1 mg/ml $MgCl_2$, 1 mg/ml Lysozyme, 1 mM PMSF) and lysed by sonication on ice. Cell lysate was centrifuged 40′ at 12000 rpm and the proteins was purified by affinity chromatography using a HisTrap column (GE Healthcare) loaded with Ni^{2+} and equilibrated with Buffer A (10 mM Hepes pH 7.5, 300 mM NaCl, 5% Glycerol). Elution was carried out by increasing the imidazole concentration, with the protein eluting at 300 mM imidazole. Fractions containing pure protein were analysed through SDS-page and collected. Imidazole was removed with PD-10 desalting columns (GE Healthcare) and then the proteins were loaded on an Superdex 200 26/600 (GE Healthcare) and eluted with buffer A using FPLC apparatus (Akta system). All the purified proteins were flash frozen in liquid nitrogen and stored at − 20 °C. Samples were tested for homogeneity, purity and integrity according to published recommendations (Das et al., 2015; Raynal et al., 2021).

FAD quantification of cRmcA long and mutants was obtained by adding 1uL of Proteinase K (Sigma Merck) at each protein sample. After 1 h, samples were boiled for 10′, centrifugated for 10′ and quantified by absorbance spectrum using absorbance value at 446 nm (cRmcA ε_{280} = 104655 $M^{-1}cm^{-1}$; FAD ε_{446} = 11.7 $mM^{-1}cm^{-1}$; *P. putida* cRmcA ε_{280} = 103540 $M^{-1}cm^{-1}$).

Kinetic assays: The kinetic assays were carried out in 10 mM Hepes pH 8.0, 300 mM NaCl, 5% Glycerol 2.5 mM $MnCl_2$. PDE activity was analyzed by real-time kinetics using circular dichroism (CD), as previously published (Stelitano et al., 2013). Most of the assays carried out with the wildtype proteins and its mutants were done starting from a solution containing 450 μl of 30 μM c-di-GMP (BioLog), 100 μM GTP and, if indicated, 50 μM FAD (Sigma Merck) in kinetic buffer put in 1-cm path quartz cuvette (Hellma); CD signal was then followed at 282 nm using a JASCO J-710 spectropolarimeter at 25 °C. After 60 s, 50 μl of protein solution pre-incubated 10 min with 100 μM GTP and, if indicated 50 μM FAD was added. C-di-GMP degradation was monitored for at least 10 min. If indicated, different FAD and/or c-di-GMP were assayed. The final cRmcA concentration was 0.15 μM with the exception of the Y768A mutant, which was 0.3 μM.

Kinetic assays in hypoxic conditions were performed under N_2 atmosphere. C-di-GMP mixture (900 μl) and protein solution (90 μl) were prepared in septa-sealed glass vials and were equilibrated at room temperature with N_2, for 5 min and 1 min, respectively. $FADH_2$ was obtained by adding 500 μM of dithionite (Emsure). To obtain dithionite solution, the powder was equilibrated with N_2 for 10 min and then dissolved in 100 mM Hepes pH 8.0 (N_2 flushed) to prepare a 200 mM solution; diluted solution (5 mM) was freshly prepared for each kinetic assay, by diluting the 200 mM solution with degassed buffer. The assays were performed as described above, in 1-cm path sealed quartz cuvette previously equilibrated with N_2 for 3 min. All the solutions were transferred using gas-tight Hamilton syringes. These conditions were optimal to avoid $FADH_2$ oxidation within the timeframe of the kinetics, by keeping at minimum possible spectral and chemical interference of dithionite with nucleotides. *P. putida* cRmcA was assayed under hypoxic conditions with GTP, GTP+FAD, GTP+$FADH_2$ and 0.15 μM enzyme.

The values are the means of data from at least four independent experiments, and the errors are ± SD. Statistical differences were determined by Anova followed by Bonferroni posthoc test. $P \leq 0.01$ was considered significant.

4.1. Binding of fluorescent GTP

Titration of cRmcA with MANT-GTP (BioLog) was assayed on a Fluoromax single photon counting spectrofluorometer (Horiba JobinYvon). Experiments were performed in 10 mM Hepes pH 8.0, 300 mM NaCl, 5% Glycerol 2.5 mM $CaCl_2$ at 25 °C in a final volume of 500 μl. Proteins solution (1 μM) were preincubated with and without 50 μM FAD and titrated with MANT-GTP at increasing concentrations; fluorescence spectra were collected after three minutes upon MANT-GTP addition to protein solution and were then baseline corrected by subtracting the buffer from the raw data. Protein tryptophanes were excited

at 280 nm and the fluorescence emission spectra were recorded between 400 and 550 nm, as a result of Förster resonance energy transfer (FRET) from excited tryptophanes to MANT-GTP in 1-cm light path cuvette (Hellma).

4.2. Dynamic light scattering (DLS)

The effective hydrodynamic diameter (DH) of protein samples was evaluated using the Zetasizer Nano S (Malvern Instruments, Malvern, UK) equipped with a 4 mW He-Ne laser 633 nm. Experiments were done with a 10 μM cRmcA solution in 2,5 mM $CaCl_2$, 300 mM NaCl, 10 mM HEPES pH 7.5. Each spectrum was collected from independent preparation in the presence of excess nucleotides, as indicated, and repeated after 15 min to ensure that no changes over the time have occurred. Measurements were carried out in MADLS (Multi-Angle Dynamic Light Scattering) mode at 25 °C with an equilibrium time of 120 s. Analysis were performed with a low volume quartz batch cuvette (ZEN2112) which contains 50 μl of final volume. Each measurement was the average of a different number of subs runs automatically determined, each being averaged for 10 s

Analytical ultracentrifugation (AUC) Samples were centrifuged at 42,000 rpm in an Optima AUC analytical ultracentrifuge (Beckman Coulter), at 20 °C in an eight-hole AN 50–Ti rotor equipped with 12-mm double-sector aluminum epoxy centerpieces. The concentrations of the individual macromolecules were chosen to be detectable by the AUC equipment without saturating the detectors.

Detection of the biomolecule concentration as a function of radial position and time was performed by absorbance measurements at different wavelengths depending of samples and buffers (see table SIII) and by interference detection. Ultracentrifugation experiments were performed in 10 mM HEPES pH7.4 300 mM NaCl with or without addition of components (see table S4). Sedimentation velocity data analysis was performed by continuous size distribution analysis c(s) using Sedfit 16.36 software (Schuck et al., 2000). All the c(s) distributions were calculated with a fitted fractional ratio f/f0 and a maximum entropy regularization procedure with a confidence level of 0.95. For the experiment performed with saturated amount of FAD, sedimentation profile was analyzed using 449 nm absorbance (specific of FAD absorption) and 288/289 nm absorbance (specific of cRmca and FAD). Peak in the c(s) distributions were integrated to estimate the amount of FAD and protein in the detected peaks using the Beer-Lambert laws. Buffer viscosity and density were calculated from the Sednterp software. Partial specific volume of cRmcA (0.736 ml/g) was also determined with Sednterp.

4.3. Native MS analysis

Protein samples were buffer exchanged into 200 mM ammonium acetate (pH 7.0) through dialysis prior to native MS analyses. These samples were directly introduced into the mass spectrometer using gold-coated capillary needles prepared in-house (Hernández and Robinson, 2007). Data were collected on a Q Exactive UHMR Hybrid Quadrupole-Orbitrap mass spectrometer (Thermo Fisher) in positive polarity. The instrument parameters used for MS spectra collection were the following: capillary voltage 1.2 kV, scan range from 2000 to 20, 000 m/z, HCD collision energy 0 V, source fragmentation 0 V, in-source trapping − 80 V. The ion transfer optics was set as follows: injection flatapole 5 V, inter-flatapole lens 4 V, bent flatapole 2 V, transfer multipole 0 V. The resolution of the instrument was 17,500 at $m/z = 200$ (transient time of 64 ms), nitrogen pressure in the HCD cell was maintained at approximately at $4.5 \times 10 - 10$ mbar and source temperature was kept at 200 °C. The noise level was set at 3 rather than the default value of 4.64. Calibration of the instrument was performed using 10 mg/ml solution of caesium iodide in water. Data were analysed using the Xcalibur 3.0 (Thermo Scientific), NaViA (Quetschlich et al., 2021), and UniDec (Marty et al., 2015) software packages.

4.4. Modeling of the RmcA PASd domain (residues 681-801)

The protein sequence of RmcA was obtained from Uniprot (ID: Q9I5W1_PSEAE; The Uniprot Consortium, 2021). Protein domain analysis was carried out using HMMscan, as implemented in PyMod3 plugin (Janson and Paiardini, 2021). A database search for homologous proteins with known three-dimensional structures returned several Light, Oxygen or Voltage (LOV) domains belonging to the PAS superfamily, including the crystal structure of the FAD-containing PAS domain of the protein NifL from *Azotobacter vinelandiia* (PDB code 2GJ3, sequence identity: 41%; E-value: 6e-21, Key et al., 2007) and the structure of the redox sensor domain of *Methylococcus capsulatus* Mmos (PDB code 3EWK, sequence identity: 33%; E-value: 3e-14, Ukaegbu and Rosenzweig, 2009), which we used as structural templates to model the PASd domain (residues 681–801) of RmcA.

4.5. Construction of the P. aeruginosa RmcA N760A mutant and colony biofilm morphology assay

Strains with point mutations were created as described in (Okegbe et al., 2017). Briefly, two ~1-kb regions flanking the site to be mutated were amplified by PCR, using primers that introduced the desired mutation. The PCR fragments were incorporated into the pMQ30 plasmid using yeast gap-repair cloning (Shanks et al., 2006). The resulting plasmid was transformed into E. coli BW29427, then into *P. aeruginosa* PA14 wild type or Δphz by biparental conjugation. PA14 single recombinants were selected on LB agar containing 100 μg/ml gentamicin. Point mutants were generated by selecting for double recombinants on agar-solidified medium containing 10% sucrose. Double recombinant genotypes were confirmed by PCR and sequencing.

For colony morphology assays, 1% tryptone plus 1% agar was autoclaved, cooled to 60 °C, and 40 μg/ml Congo red (Alfa Aesar) and 20 μg/ml Coomassie blue (OmniPur; MilliporeSigma) dyes were added to the medium. The mixture was poured into plates (100 mm by 100 mm by 15 mm; LDP) at 60 ml per plate and left to cool and solidify overnight (14–24 h) at room temperature (25 °C). Overnight liquid cultures were grown in lysogeny broth (LB) at 37 °C with shaking at 250 rpm for 12–16 h. Overnight cultures were diluted 1:100 in fresh LB, and subcultures were grown to midexponential phase (an optical density of 0.4–0.6). Colony biofilms were seeded by spotting 10 μl of this bacterial subculture onto colony morphology medium. Spots were dried and incubated at 25 °C. Biofilm development was monitored by taking images at 24-h intervals using a Keyence VHX-1000 microscope. Images shown are representative of at least 3 biological replicates.

The authors confirm that the data supporting the findings of this study are available within the article and its Supplementary materials. The data that support the findings of this study are available from the corresponding author, [SR], upon reasonable request.

CRediT authorship contribution statement

Chiara Scribani Rossi, Kelly Eckartt, Elisabetta Scarchilli, Simone Angeli: Methodology, Investigation, Validation. **Adele Di Matteo:** Methodology. **Francesca Cutruzzolà:** Resources. **Alessio Paone**: Formal analysis. **Maelenn Chevreuil, Bertrand Raynal:** Methodology, Investigation, Validation (AUC); **Francesco Fiorentino, Dante Rotili, Antonello Mai:** Methodology, Investigation, Validation. **Alessandro Arcovito and Noah Giacon:** Methodology, Investigation, Validation. **Manuel Espinosa-Urgel:** Resources. **Alexa Price-Whelan and Lars E.P. Dietrich**: Investigation, Validation, Writing – review & editing. **Alessandro Paiairdini:** Methodology, Investigation, Validation, Writing – review & editing. **Serena Rinaldo:** Methodology, Investigation, Validation, Writing – original draft, Writing – review & editing, Funding acquisition.

Declaration of Competing Interest

The authors declare that they have no known competing financial interests or personal relationships that could have appeared to influence the work reported in this paper.

Data Availability

Data will be made available on request.

Acknowledgments

The authors would like to acknowledge Sapienza University of Rome [RM120172A7AD98EB to SR, RM1221815D52AB32 to APaiardini and AR12117A63EE6037; AR2221816C44C7B3 to CSR] for financial support. AUC experiments have received funding from the European Union's Horizon 2020 research and innovation programme under grant agreement No 101004806. We thank Patrick England of the Plateforme de Biophysique Moléculaire of the C2RT (Institut Pasteur) for fruitful discussion.

Appendix A. Supporting information

Supplementary data associated with this article can be found in the online version at doi:10.1016/j.micres.2023.127498.

References

Almblad, H., Randall, T., Liu, F., Leblanc, K., Groves, R.A., Kittichotirat, W., Winsor, G.L., Fournier, N., Au, E., Groizeleau, J., Rich, J.D., Lou, Y., Granton, E., Jennings, L.K., Singletary, L.A., Winstone, T.M.L., Good, N.M., Bumgarner, R.E., Hynes, M.F., Singh, M., Stietz, M.S., Brinkman, F.S.L., Kumar, A., Brassinga, A.K.C., Parsek, M.R., Tseng, B.S., Lewis, I.A., Yipp, B.G., MacCallum, J.L., Harrison, J.J., 2021. Bacterial cyclic diguanylate signaling networks sense temperature. Nat. Commun. 12, 1986.

An, S., Wu, J., Zhang, L.H., 2010. Modulation of pseudomonas aeruginosa biofilm dispersal by a cyclic-di-gmp phosphodiesterase with a putative hypoxia-sensing domain. Appl. Environ. Microbiol 76, 8160–8173.

Becker, D.F., Zhu, W., Moxley, M.A., 2011. Flavin redox switching of protein functions. Antioxid. Redox Signal 14, 1079–1091.

Benarroch, J.M., Asally, M., 2020. The microbiologist's guide to membrane potential dynamics. Trends Microbiol 28.

Bittner, A.N., Kriel, A., Wang, J.D., 2014. Lowering GTP level increases survival of amino acid starvation but slows growth rate for Bacillus subtilis cells lacking (p)ppGpp. J. Bacteriol. 196, 2067–2076.

Chiaverotti, T.A., Parker, G., Gallant, J., Agabian, N., 1981. Conditions that trigger guanosine tetraphosphate accumulation in Caulobacter crescentus. J. Bacteriol. 145, 1463–1465.

Commichau, F.M., Forchhammer, K., Stülke, J., 2006. Regulatory links between carbon and nitrogen metabolism. Curr. Opin. Microbiol 9, 167–172.

Das, T., Kutty, S., Tavallaie, R., Ibugo, A.I., Panchompoo, J., Sehar, S., Aldous, L., Yeung, A.W.S., Thomas, S.R., Kumar, N., Gooding, J.J., Manefield, M., 2015. Phenazine virulence factor binding to extracellular DNA is important for Pseudomonas aeruginosa biofilm formation. Sci. Rep. 5, 8398.

Dietrich, L.E.P., Okegbe, C., Price-Whelan, A., Sakhtah, H., Hunter, R.C., Newmana, D.K., 2013. Bacterial community morphogenesis is intimately linked to the intracellular redox state. J. Bacteriol. 195, 1371–1380.

Fiorentino, F., Rotili, D., Mai, A., Bolla, J.R., Robinson, C.V., 2021. Mass spectrometry enables the discovery of inhibitors of an LPS transport assembly via disruption of protein–protein interactions. Chem. Commun. 57, 10747–10750.

Fiorentino, F., Rotili, D., Mai, A., 2023. Native mass spectrometry-directed drug discovery: recent advances in investigating protein function and modulation. Drug Discov. Today 28, 103548.

Garcia, D., Watts, K.J., Johnson, M.S., Taylor, B.L., 2016. Delineating PAS-HAMP interaction surfaces and signalling-associated changes in the aerotaxis receptor Aer. Mol. Microbiol 100, 156–172.

Giardina, G., Castiglione, N., Caruso, M., Cutruzzolà, F., Rinaldo, S., 2011. The Pseudomonas aeruginosa DNR transcription factor: light and shade of nitric oxide-sensing mechanisms. Biochem Soc. Trans. 39, 294–298.

Gupta, S., Laskar, N., Kadouri, D.E., 2016. Evaluating the effect of oxygen concentrations on antibiotic sensitivity, growth, and biofilm formation of human pathogens. Microbiol Insights 9.

Ha, D.-G., O'Toole, G.A., 2015. c-di-GMP and its effects on biofilm formation and dispersion: a pseudomonas aeruginosa review, 2165–0497 Microbiol Spectr. 3, 2165–0497.

Hansson, M.D., Rzeznicka, K., Rosenbäck, M., Hansson, M., Sirijovski, N., 2008. PCR-mediated deletion of plasmid DNA. Anal. Biochem 375, 373–375.

Harrison, J.J., Parsek, M.R., Tseng, B.S., 2021. Bacterial adaptation in structured environments: lessons from Darwin's Finches. Trends Microbiol 29, 5–7.

Heikal, A.A., 2010. Intracellular coenzymes as natural biomarkers for metabolic activities and mitochondrial anomalies. Biomark. Med 4, 241–263.

Hengge, R., 2021. High-specificity local and global c-di-GMP signaling. Trends Microbiol 29, 993–1003.

Hernández, H., Robinson, C.V., 2007. Determining the stoichiometry and interactions of macromolecular assemblies from mass spectrometry. Nat. Protoc. 2, 715–726.

Hilser, V.J., Anderson, J.A., Motlagh, H.N., 2015. Allostery vs. "allokairy. Proc. Natl. Acad. Sci. USA 112, 11430–11431.

Janson, G., Paiardini, A., 2021. PyMod 3: A complete suite for structural bioinformatics in PyMOL. Bioinformatics 37, 1471–1472.

Jo, J., Cortez, K.L., Cornell, W.C., Price-Whelan, A., Dietrich, L.E.P., 2017. An orphan cbb3-type cytochrome oxidase subunit supports Pseudomonas aeruginosa biofilm growth and virulence. Elife 6, e30205.

Jo, J., Price-Whelan, A., Dietrich, L.E.P., 2022. Gradients and consequences of heterogeneity in biofilms. Nat. Rev. Microbiol 20, 593–607.

Kahl, L.J., Price-Whelan, A., Dietrich, L.E.P., 2020. Light-mediated decreases in cyclic di-GMP levels inhibit structure formation in pseudomonas aeruginosa biofilms. J. Bacteriol. 202, e00117–e00120.

Katharios-Lanwermeyer, S., Whitfield, G.B., Howell, P.L., O'toole, G.A., 2021. Pseudomonas aeruginosa uses c-di-gmp phosphodiesterases rmca and mora to regulate biofilm maintenance. mBio 12 (1), 19.

Kawashima, S.A., Takemoto, A., Nurse, P., Kapoor, T.M., 2013. A chemical biology strategy to analyze rheostat-like protein kinase-dependent regulation. Chem. Biol. 20, 262–271.

Krasteva, P.V., Sondermann, H., 2017. Versatile modes of cellular regulation via cyclic dinucleotides. Nat. Chem. Biol. 13, 350–359.

Little, R., Slavny, P., Dixon, R., 2012. Influence of PAS domain flanking regions on oligomerisation and redox signalling By NifL. PLoS One 7, e46651.

Liu, C., Liew, C.W., Wong, Y.H., Tan, S.T., Poh, W.H., Manimekalai, M.S.S., Rajan, S., Xin, L., Liang, Z.X., Grüber, G., Rice, S.A., Lescar, J., 2018. Insights into biofilm dispersal regulation from the crystal structure of the PAS-GGDEF-EAL region of RbdA from pseudomonas aeruginosa. J. Bacteriol. 200, e00515–e00517.

Lopez, J.M., Dromerick, A., Freese, E., 1981. Response of guanosine 5′-triphosphate concentration to nutritional changes and its significance for Bacillus subtilis sporulation. J. Bacteriol. 146, 605–613.

Mantoni, F., Paiardini, A., Brunotti, P., D'Angelo, C., Cervoni, L., Paone, A., Cappellacci, L., Petrelli, R., Ricciutelli, M., Leoni, L., Rampioni, G., Arcovito, A., Rinaldo, S., Cutruzzolà, F., Giardina, G., 2018. Insights into the GTP-dependent allosteric control of c-di-GMP hydrolysis from the crystal structure of PA0575 protein from Pseudomonas aeruginosa. FEBS J 285, 3815–3834.

Marty, M.T., Baldwin, A.J., Marklund, E.G., Hochberg, G.K.A., Benesch, J.L.P., Robinson, C.V., 2015. Bayesian deconvolution of mass and ion mobility spectra: from binary interactions to polydisperse ensembles. Anal. Chem. 87, 4370–4376.

Meinhardt, S., Manley, M.W., Parente, D.J., Swint-Kruse, L., 2013. Rheostats and toggle switches for modulating protein function. PLoS One 8, e83502.

Navarro, M.V.A.S., Newell, P.D., Krasteva, P.V., Chatterjee, D., Madden, D.R., O'Toole, G.A., Sondermann, H., 2011. Structural basis for c-di-GMP-mediated inside-out signaling controlling periplasmic proteolysis. PLoS Biol 9, e1000588.

Okegbe, C., Fields, B.L., Cole, S.J., Beierschmitt, C., Morgan, C.J., Price-Whelan, A., Stewart, R.C., Lee, V.T., Dietrich, L.E.P., 2017. Electron-shuttling antibiotics structure bacterial communities by modulating cellular levels of c-di-GMP. Proc. Natl. Acad. Sci. 114, 6661.

Orr, M.W., Donaldson, G.P., Severin, G.B., Wang, J.S., Sintim, H.O., Waters, C.M., Lee, V. T., 2015. Oligoribonuclease is the primary degradative enzyme for pGpG in Pseudomonas aeruginosa that is required for cyclic-di-GMP turnover. Proc. Natl. Acad. Sci. USA 112, E5048–E5057.

Paiardini, A., Mantoni, F., Giardina, G., Paone, A., Janson, G., Leoni, L., Rampioni, G., Cutruzzolà, F., Rinaldo, S., 2018. A novel bacterial l-arginine sensor controlling c-di-GMP levels in Pseudomonas aeruginosa. Protein.: Struct., Funct., Bioinforma. 86, 1088–1096.

Pierson, L.S., Pierson, E.A., 2010. Metabolism and function of phenazines in bacteria: Impacts on the behavior of bacteria in the environment and biotechnological processes. Appl. Microbiol Biotechnol. 86, 1659–1670.

Price-Whelan, A., Dietrich, L.E.P., Newman, D.K., 2007. Pyocyanin alters redox homeostasis and carbon flux through central metabolic pathways in Pseudomonas aeruginosa PA14. J. Bacteriol. 189, 6372–6381.

Qi, Y., Rao, F., Luo, Z., Liang, Z.X., 2009. A flavin cofactor-binding PAS domain regulates c-di-GMP synthesis in AxDGC2 from Acetobacter xylinum. Biochemistry 48, 10275–10285.

Quetschlich, D., Esser, T.K., Newport, T.D., Fiorentino, F., Shutin, D., Chen, S., Davis, R., Lovera, S., Liko, I., Stansfeld, P.J., Robinson, C.V., 2021. NaViA: a program for the visual analysis of complex mass spectra. Bioinformatics 37, 4876–4878.

Randall, T.E., Eckartt, K., Kakumanu, S., Price-Whelan, A., Dietrich, L.E.P., Harrison, J.J., 2022. Sensory perception in bacterial cyclic diguanylate signal transduction. J. Bacteriol. 204, e00433–21.

Rao, F., Qi, Y., Chong, H.S., Kotaka, M., Li, B., Li, J., Lescar, J., Tang, K., Liang, Z.X., 2009. The functional role of a conserved loop in EAL domain-based cyclic di-GMP-specific phosphodiesterase. J. Bacteriol. 191, 4722–4731.

Raynal, B., Brûlé, S., Uebel, S., Knauer, S.H., 2021. Assessing and improving protein sample quality. Methods Mol. Biol. 3–46.

Rinaldo, S., Paiardini, A., Stelitano, V., Brunotti, P., Cervoni, L., Fernicola, S., Protano, C., Vitali, M., Cutruzzolà, F., Giardina, G., 2015. Structural basis of functional diversification of the HD-GYP domain revealed by the Pseudomonas

aeruginosa PA4781 protein, which displays an unselective bimetallic binding site. J. Bacteriol. 197, 1525–1535.
Römling, U., Liang, Z.-X., Dow, J.M., 2017. Progress in understanding the molecular basis underlying functional diversification of cyclic dinucleotide turnover proteins. J. Bacteriol. 199, e00790–16.
Ruggiero, M.J., Malhotra, S., Fenton, A.W., Swint-Kruse, L., Karanicolas, J., Hagenbuch, B., 2022. Structural plasticity is a feature of rheostat positions in the human Na+/taurocholate cotransporting polypeptide (NTCP). Int J. Mol. Sci. 23, 3211.
Samanta, D., Widom, J., Borbat, P.P., Freed, J.H., Crane, B.R., 2016. Bacterial energy sensor aer modulates the activity of the chemotaxis kinase CheA based on the redox state of the flavin cofactor. J. Biol. Chem. 291, 25809–25814.
Saunders, S.H., Tse, E.C.M., Yates, M.D., Otero, F.J., Trammell, S.A., Stemp, E.D.A., Barton, J.K., Tender, L.M., Newman, D.K., 2020. Extracellular DNA PRomotes Efficient Extracellular Electron Transfer by Pyocyanin in Pseudomonas Aeruginosa Biofilms. Cell 182, 919–932.e19.
Schuck, P., 2000. Size-distribution analysis of macromolecules by sedimentation velocity ultracentrifugation and Lamm equation modeling. Biophys. J. 78, 1606–1619.
Scribani Rossi, C., Barrientos-Moreno, L., Paone, A., Cutruzzolà, F., Paiardini, A., Espinosa-Urgel, M., Rinaldo, S., 2022. Nutrient Sensing and Biofilm Modulation: The Example of L-arginine in Pseudomonas. Int J. Mol. Sci., 234386
Sen, C.K., Mathew-Steiner, S.S., Das, A., Sundaresan, V.B., Roy, S., 2020. Electroceutical management of bacterial biofilms and surgical infection. Antioxid. Redox Signal 33.
Shanks, R.M.Q, Caiazza, N.C., Hinsa, S.M., Toutain, C., O'Toole, G.A., 2006. Saccharomyces cerevisiae-based molecular tool kit for manipulation of genes from gram-negative bacteria. Appl. Environ. Microbiol 72, 5027–5036.
Shcherbakova, D.M., Shemetov, A.A., Kaberniuk, A.A., Verkhusha, V.v, 2015. Natural photoreceptors as a source of fluorescent proteins, biosensors, and optogenetic tools. Annu Rev. Biochem 84, 519–550.
Sporer, A.J., Kahl, L.J., Price-Whelan, A., Dietrich, L.E.P., 2017. Redox-based regulation of bacterial development and behavior. Annu Rev. Biochem 86, 777–797.
Stelitano, V., Brandt, A., Fernicola, S., Franceschini, S., Giardina, G., Pica, A., Rinaldo, S., Sica, F., Cutruzzolà, F., 2013. Probing the activity of diguanylate cyclases and c-di-GMP phosphodiesterases in real-time by CD spectroscopy e79–e79 Nucleic. Acids Res 41, e79.
Urién, C., Chopo-Escuin, G., Tommassen, J., Mainar-Jaime, R.C., Arenas, J., 2021. Biofilms as promoters of bacterial antibiotic resistance and tolerance. Antibiotics 10.
Wu, T., Swint-Kruse, L., Fenton, A.W., 2019. Functional tunability from a distance: Rheostat positions influence allosteric coupling between two distant binding sites. Sci. Rep. 9, 16957.
Yalcin, S.E., Malvankar, N.S., 2020. The blind men and the filament: understanding structures and functions of microbial nanowires. Curr. Opin. Chem. Biol. 59, 193–201.